CHAPTER III

RESULTS AND DISCUSSION

The hexadentate Schiff base metal complexes were synthesized from the literature.[33] The reaction between salicylaldehyde derivatives and metal (II) acetate in methanol to form a template intermediate. Subsequently, the solution of triethylenetetramine was then added to obtain $M(Sal)_2trien$ and $M(XSal)_2trien$ (Scheme 3.1).

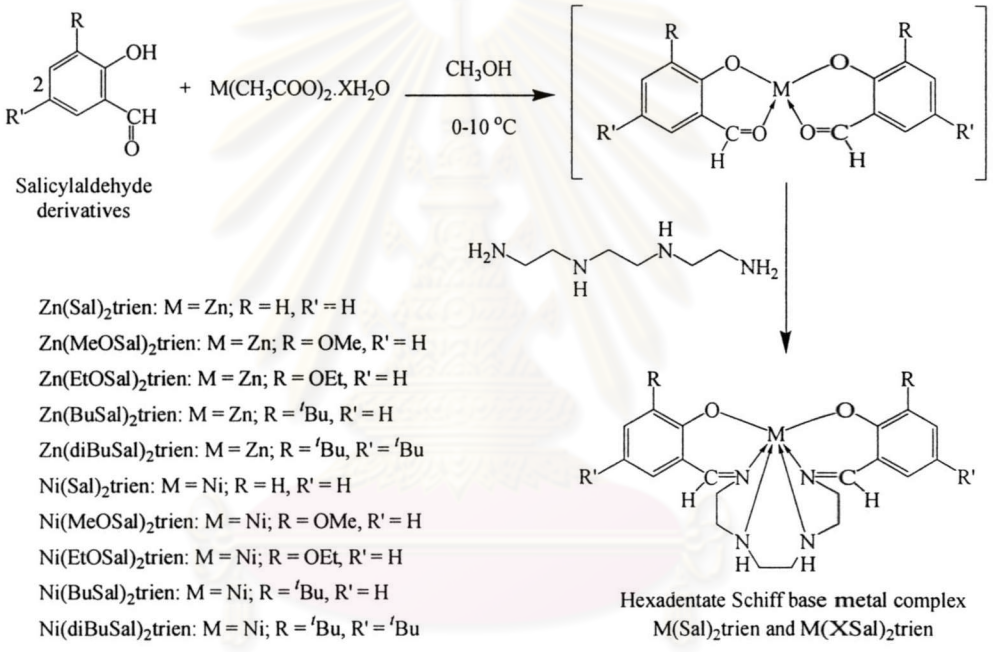

Scheme 3.1 Synthesis of Schiff base metal complexes.

3.1 Synthesis of hexadentate Schiff base zinc complexes

3.1.1 Characterization of hexadentate Schiff base zinc complexes

$Zn(Sal)_2trien$ were synthesized and the spectroscopic data was in good agreement with those reported in the literature.[33] $Zn(XSal)_2trien$ was also synthesized by a one-pot reaction by adding triethylenetetramine to a mixture of metal acetates and salicylaldehyde derivatives, namely 3-methoxysalicylaldehyde, 3-ethoxysalicylaldehyde, 3-*tert*-butyl-2-hydroxybenzaldehyde and 3,5-di-*tert*-butyl-2-hydroxybenzaldehyde. The purpose of $Zn(XSal)_2trien$ synthesis was to increase solubility of the metal complex in various organic solvents. Like $Zn(Sal)_2trien$, all

$Zn(XSal)_2trien$ were also soluble in many organic solvents such as dichloromethane, acetone and methanol. The order of solubility of zinc complexes in solvents is $Zn(EtOSal)_2trien$ > $Zn(Sal)_2trien$ > $Zn(BuSal)_2trien$ = $Zn(diBuSal)_2trien$ > $Zn(MeOSal)_2trien$.

The structure of $Zn(Sal)_2trien$ and $Zn(XSal)_2trien$ was confirmed by IR, NMR, MS and elemental analysis. IR spectra (Figure 3.1 and Tables 3.1) of the zinc complexes showed important bands of C=N stretching between 1632 and 1648 cm^{-1}. ^1H and ^{13}C NMR data (Figures A.6-A.8) also support their structures. ^1H NMR spectra (Figures A.1-A.5 and Tables 3.1) showed the imine -CH=N- protons and carbons of $Zn(Sal)_2trien$ and $Zn(XSal)_2trien$ around δ 8.13-8.23 and δ 166-168, respectively. FAB MS data of all zinc complexes (Table 3.3) gave the corresponding molecular formula.

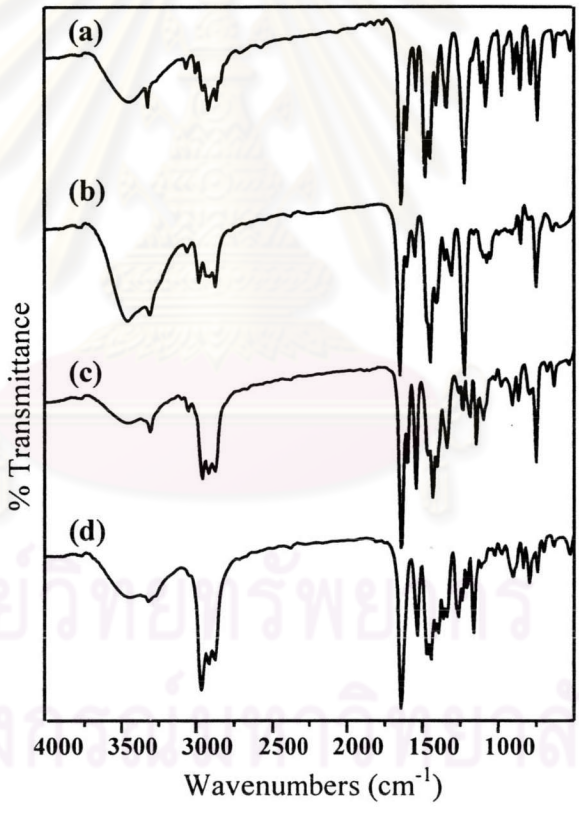

Figure 3.1 IR spectra of (a) $Zn(MeOSal)_2trien$; (b) $Zn(EtOSal)_2trien$; (c) $Zn(BuSal)_2trien$; (d) $Zn(diBuSal)_2trien$

Table 3.1 IR and ^{1}H NMR data of zinc complexes

Zinc Complexes	IR (cm^{-1})			^{1}H NMR (ppm)				
	ν_{NH}	$\nu_{CH=N}$	$\nu_{C=C}$	CH=N	Aromatic	N-H	Methylene groups	Functional groups
$Zn(Sal)_2trien$	3646	1634	1600	8.13	7.15 (*t*, 2H), 7.06 (*d*, 2H), 6.74 (*d*, 2H), 6.45 (*t*, 2H)	4.71-4.75	4.05-4.29 (*m*, 2H), 3.21-3.48 (*m*, 4H), 2.73-2.92 (*m*, 2H), 2.35-2.61 (*m*, 4H)	-
$Zn(MeOSal)_2trien$	3428	1632	1598	8.25	6.69 (*dd*, 2H), 6.62 (*dd*, 2H), 6.14 (*t*, 2H)	3.78-3.84	-	3.59 (*s*, 6H)
$Zn(EtOSal)_2trien$	3446	1642	1596	8.12	6.66 (*d*, 2H), 6.64 (*d*, 2H), 6.21 (*t*, 2H)	4.16-4.20	3.25-3.27 (*m*, 4H), 2.82-2.84 (*m*, 2H), 2.41-2.45 (*m*, 4H), 2.17 (*m*, 2H)	3.90-3.82 (*m*, 2H), 3.74-3.78 (*m*, 2H), 1.18-1.22 (*t*, 6H)
$Zn(BuSal)_2trien$	3440	1632	1593	8.23	7.15 (*dd*, 2H), 6.91 (*dd*, 2H), 6.33 (*t*, 2H)	4.09-4.16	3.48-3.54 (*m*, 2H), 3.36-3.43 (*m*, 2H), 3.06-3.09 (*m*, 2H), 2.64-2.73 (*m*, 4H), 2.20 (*m*, 2H)	1.32 (*s*, 18H)
$Zn(diBuSal)_2trien$	3435	1634	1528	8.23	7.25 (*d*, 2H), 6.84 (*d*, 2H)	4.29-4.35	3.32-3.39 (*m*, 4H), 2.99-3.01 (*m*, 2H), 2.54-2.64 (*m*, 4H), 2.11-2.14 (*m*, 2H)	1.37 (*s*, 18H), 1.28 (*s*, 18H)

Table 3.2 ^{13}C NMR data of zinc complexes

Zinc complexes	^{13}C NMR (ppm)			
	CH=N	Aromatic	Methylene groups	X groups
$Zn(Sal)_2trien$	168	172, 135, 133, 124, 119, 112	56, 47, 43	-
$Zn(EtOSal)_2trien$	166	164, 151, 127, 119, 117, 110	56, 47, 43	64, 15 (OEt)
$Zn(BuSal)_2trien$	167	171, 141, 133, 129, 119, 110	55, 46, 43	34, 29 (Bu)
$Zn(diBuSal)_2trien$	167	169, 140, 132, 128, 127, 117	56, 46, 43	35, 33, 31, 29 (Bu)

Table 3.3 indicates the possible molecular formulas and molecular weight of zinc complexes. Analytical data show that the experimentally determined percentage values of carbon, hydrogen and nitrogen are within the calculated values.

Table 3.3 Analytical data of zinc complexes

Zinc complexes	Formula	Analytical data found (calculated) (%)			*m/z*
		C	H	N	
$Zn(Sal)_2trien•H_2O$[33]	$C_{20}H_{24}N_4O_2Zn$ $•H_2O$	54.65 (55.12)	6.59 (6.01)	12.79 (12.79)	417.3
$Zn(MeOSal)_2trien$	$C_{22}H_{28}N_4O_4Zn$	55.05 (55.29)	5.94 (5.91)	11.74 (11.72)	477.1
$Zn(EtOSal)_2trien•CH_3OH$	$C_{24}H_{32}N_4O_4Zn$ $•CH_3OH$	55.58 (55.82)	6.85 (6.74)	10.83 (10.41)	505.2
$Zn(BuSal)_2trien$	$C_{28}H_{40}N_4O_2Zn$	63.03 (63.45)	7.57 (7.61)	10.59 (10.57)	529.3
$Zn(diBuSal)_2trien$	$C_{36}H_{56}N_4O_2Zn$	66.90 (67.32)	8.76 (8.79)	8.72 (8.72)	641.4

The structure of $Zn(MeOSal)_2trien$ was determined by X-ray crystallography. The overall view of $Zn(MeOSal)_2trien$ is shown in Figure 3.2. Bond lengths and bond angles are listed in appendix B. X-ray crystallography indicated that the structure of $Zn(MeOSal)_2trien$ is similar to that of $Zn(Sal)_2trien$.[33] Both $Zn(MeOSal)_2trien$ and $ZnSal_2trien$ has a roof-shaped structure with the slope containing benzene rings and the zinc atom that adopting a distorted octahedral geometry.

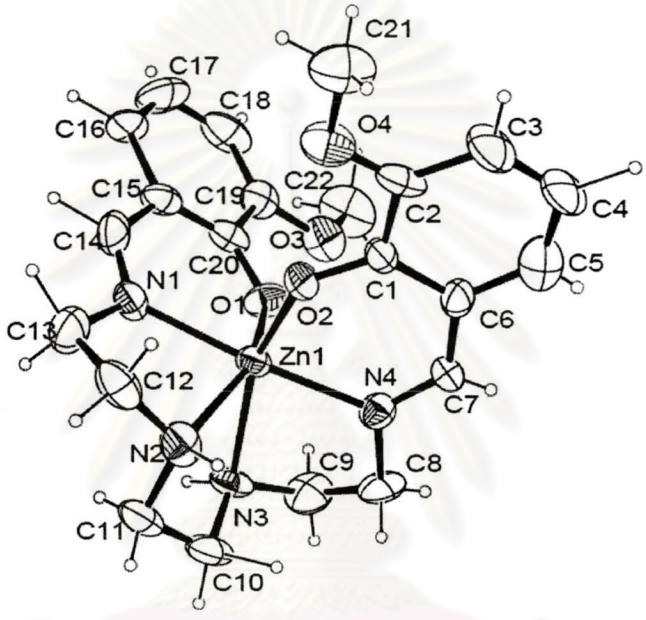

Figure 3.2 X-ray crystal structure of $Zn(MeOSal)_2trien$

3.1.2 Thermal property of zinc complexes

Thermal properties of zinc complexes were investigated using differential scanning calorimetry (DSC) and thermogravimetric analysis (TGA).

DSC thermogram of $Zn(MeOSal)_2trien$, $Zn(EtOSal)_2trien$, $Zn(BuSal)_2trien$ and $Zn(diBuSal)_2trien$ (Figures 3.3, 3.4, 3.5 and 3.6, respectively) showed endotherm peaks around 292, 238, 296 and 292 °C, respectively followed immediately by decomposition of the materials. According to these DSC endothermic peaks, $Zn(MeOSal)_2trien$, $Zn(EtOSal)_2trien$, $Zn(BuSal)_2trien$ and $Zn(diBuSal)_2trien$ did not show liquid crystalline property. $Zn(EtOSal)_2trien$ showed another endothermic peak around 83°C, which might be due to a loss of methanol.

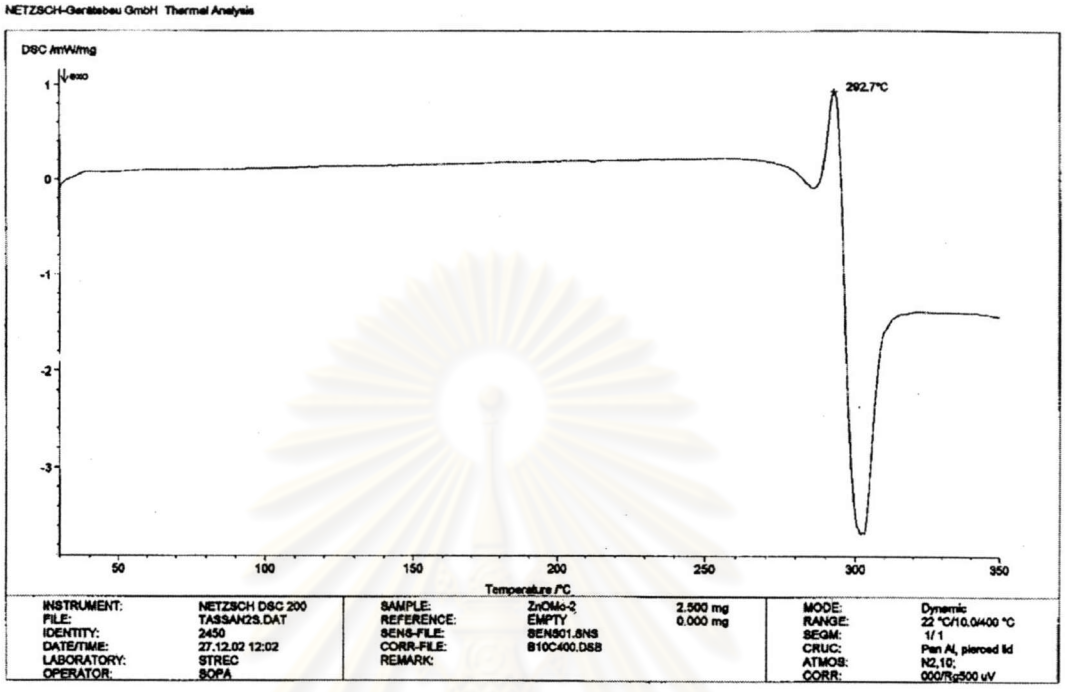

Figure 3.3 DSC thermogram of $Zn(MeOSal)_2trien$

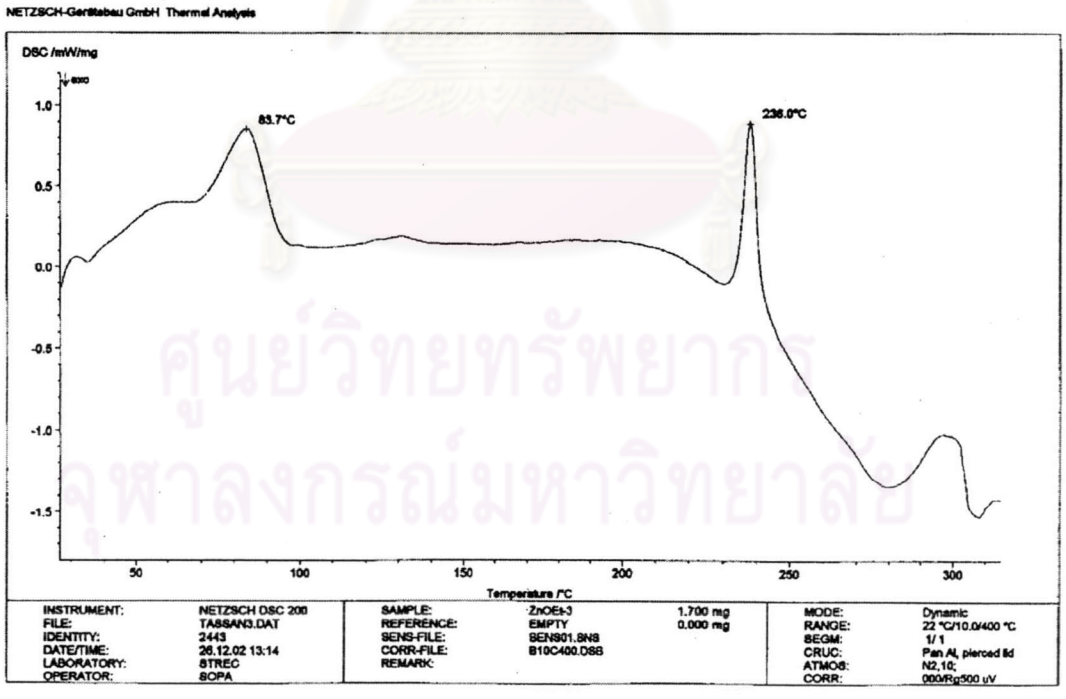

Figure 3.4 DSC thermogram of $Zn(EtOSal)_2trien$

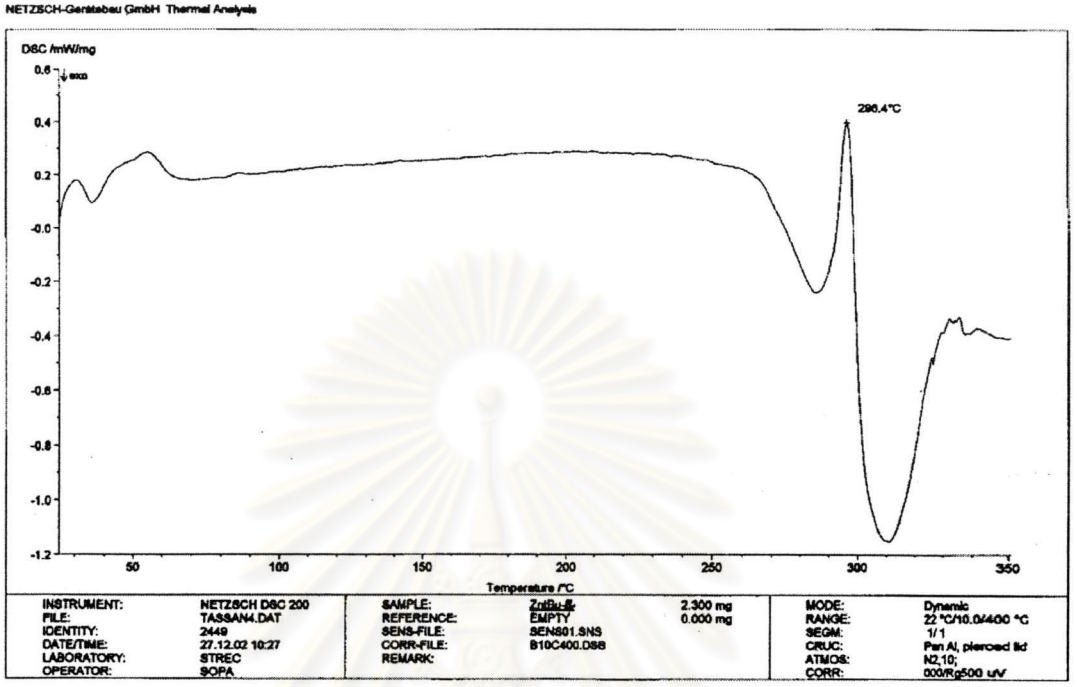

Figure 3.5 DSC thermogram of $Zn(BuSal)_2trien$

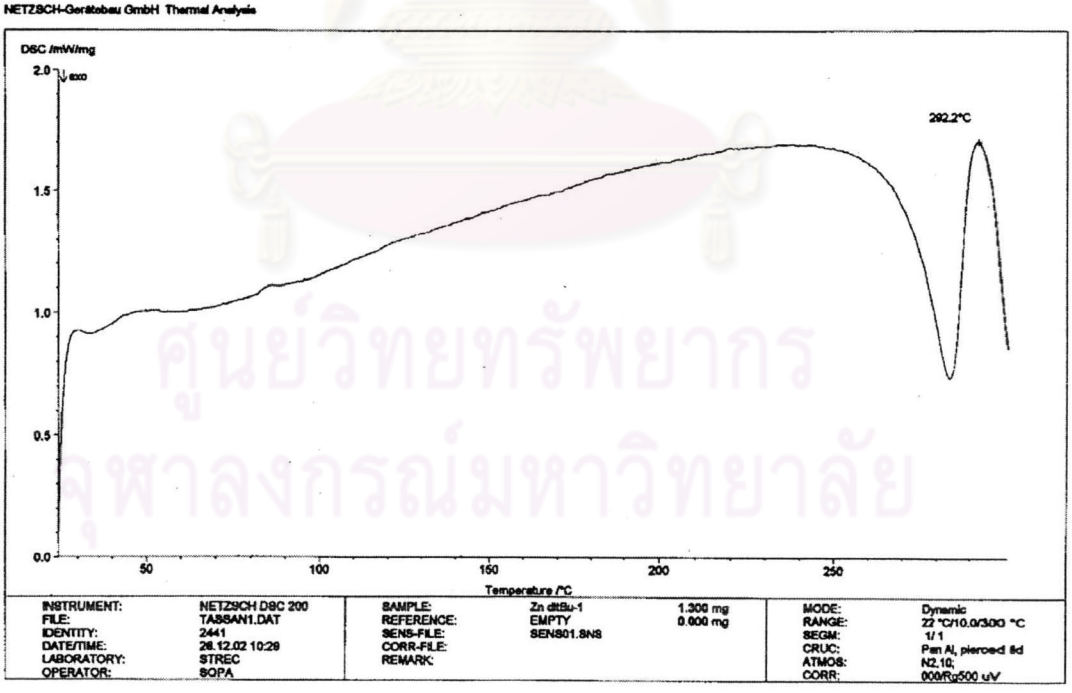

Figure 3.6 DSC thermogram of $Zn(diBuSal)_2trien$

From the above DSC data, it was found that the zinc complexes showed good thermal stability. Therefore, thermal stability of the complexes was investigated by using of TGA. TGA curves of zinc complexes are displayed in Figure 3.7. Weight loss percentages of zinc complexes at different temperatures and initial decomposition temperatures are given in Table 3.4. TGA thermograms indicated that all zinc complexes were stable up to 230 °C (The initial decomposition temperature (IDT) of the complexes was found to be in the range of 232-274°C.). For $Zn(Sal)_2trien•H_2O$ and $Zn(EtOSal)_2trien•CH_3OH$, the loss of solvent was not observed since TGA samples were heated in an oven at 80°C for 30 min before putting in the instrument. The residual weight percentages at 900°C of $Zn(Sal)_2trien$, $Zn(MeOSal)_2trien$, $Zn(EtOSal)_2trien$, $Zn(BuSal)_2trien$ and $Zn(diBuSal)_2trien$ were 20%, 17%, 18%, 16% and 16%, respectively.

Table 3.4 TGA data of zinc complexes

Zinc complexes	IDTs (°C)	Weight loss (%) at different temperature (°C)					
		300	400	500	600	700	900
$Zn(Sal)_2trien•H_2O$	248	6	19	29	56	68	80
$Zn(MeOSal)_2trien$	258	9	23	31	62	76	83
$Zn(EtOSal)_2trien•CH_3OH$	232	14	31	41	60	75	82
$Zn(BuSal)_2trien$	274	2	29	43	68	84	84
$Zn(diBuSal)_2trien$	258	3	34	52	72	84	84

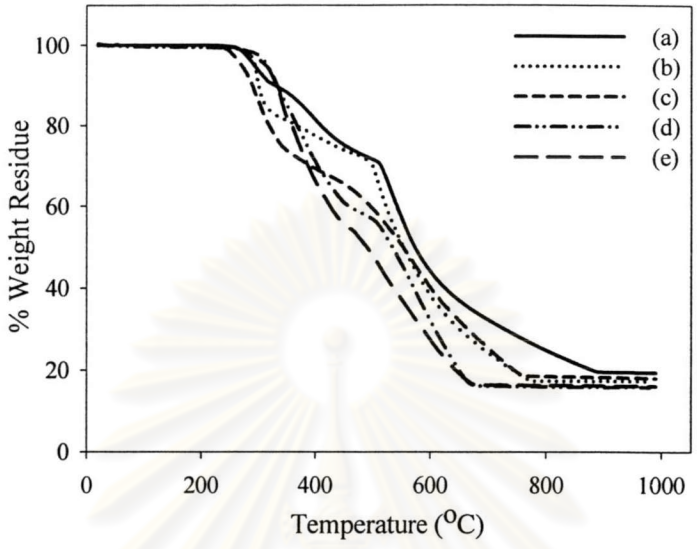

Figure 3.7 TGA thermograms of (a) $Zn(Sal)_2trien$; (b) $Zn(MeOSal)_2trien$; (c) $Zn(EtOSal)_2trien$; (d) $Zn(BuSal)_2trien$; (e) $Zn(diBuSal)_2trien$

3.2 Synthesis of hexadentate Schiff base nickel complexes

3.2.1 Characterization of hexadentate Schiff base nickel complexes

IR spectrum of $Ni(Sal)_2trien$ showed an absorption band of imine C=N stretching at 1642 cm^{-1} and aromatic C-H bending at 950 cm^{-1} which agreed with the data reported in the literature.[32] IR spectra of $Ni(MeOSal)_2trien$, $Ni(EtOSal)_2trien$, $Ni(BuSal)_2trien$ and $Ni(diBuSal)_2trien$ showed an absorption band of imine C=N stretching at 1632, 1648, 1633 and 1633 cm^{-1}, respectively. All $Ni(XSal)_2trien$ were soluble in many organic solvents such as dichloromethane, acetone and methanol. The order of solubility is $Ni(EtOSal)_2trien$ > $Ni(Sal)_2trien$ > $Ni(BuSal)_2trien$ = $Ni(diBuSal)_2trien$ > $Ni(MeOSal)_2trien$.

FAB MS data of nickel complexes (Table 3.5) gave the corresponding molecular formula. Table 3.5 indicates the possible molecular formulas and molecular weight of nickel complexes. Analytical data shows that the experimentally determined percentage values of carbon, hydrogen and nitrogen are within the calculated values.

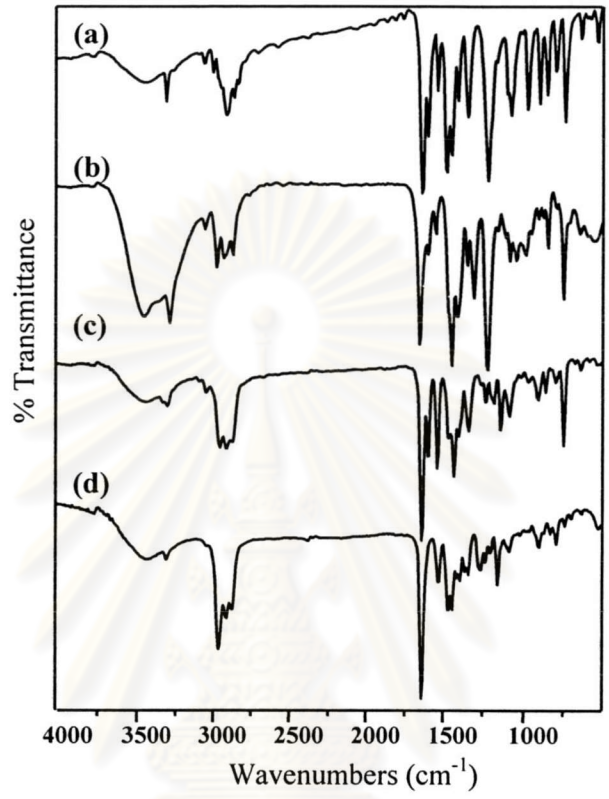

Figure 3.8 IR spectra of (a) $Ni(MeOSal)_2trien$; (b) $Ni(EtOSal)_2trien$; (c) $Ni(BuSal)_2trien$; (d) $Ni(diBuSal)_2trien$

The structure of $Ni(BuSal)_2trien$ was also determined by X-ray crystallography. Bond lengths and bond angles are listed in appendix B. Similar to zinc complexes, X-ray crystallography indicated that $Ni(BuSal)_2trien$ have roof-shaped structure with the slope containing benzene rings and the nickel atom adopting a distorted octahedral geometry.

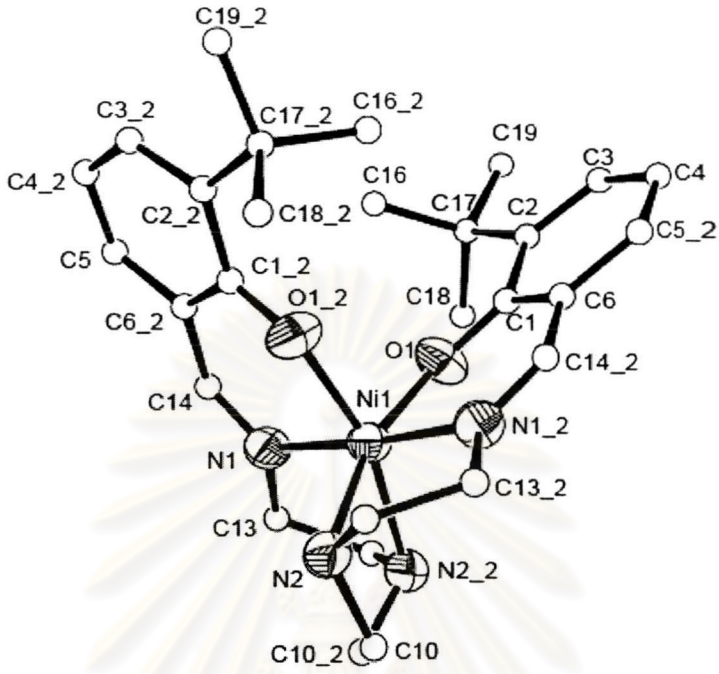

Figure 3.9 X-ray crystal structure of $Ni(BuSal)_2trien$

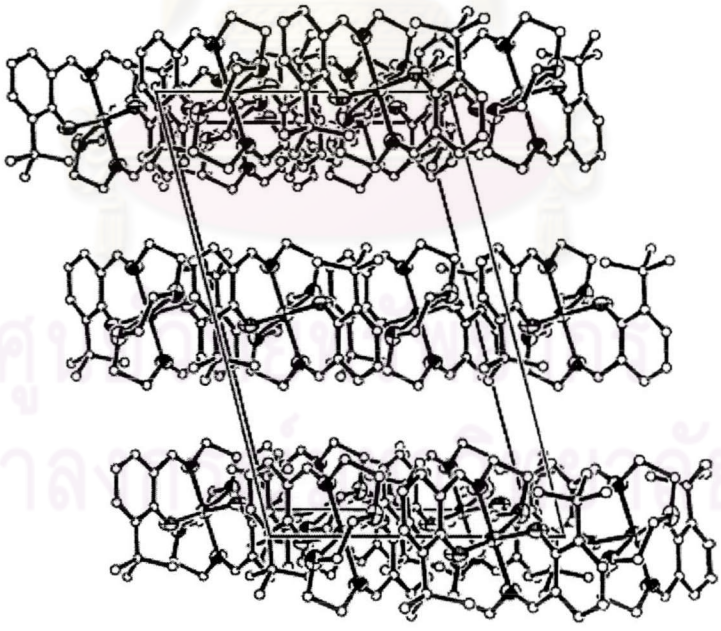

Figure 3.10 Columnar packing in the crystal structure of $Ni(BuSal)_2trien$

Table 3.5 Analytical data of nickel complexes

Nickel-complex	Formula	Analytical data found (calculated) (%)			*m/z*
		C	H	N	
$Ni(MeOSal)_2trien•H_2O$	$C_{22}H_{28}N_4O_4Ni•H_2O$	54.53 (54.01)	6.31 (6.18)	11.54 (11.45)	471.2
$Ni(EtOSal)_2trien•3H_2O$	$C_{24}H_{32}N_4O_4Ni•3H_2O$	52.76 (52.10)	7.20 (6.92)	10.73 (10.13)	499.2
$Ni(BuSal)_2trien$	$C_{28}H_{40}N_4O_2Ni$	64.24 (64.26)	7.72 (7.70)	10.78 (10.71)	523.3
$Ni(diBuSal)_2trien$	$C_{36}H_{56}N_4O_2Ni$	67.95 (68.03)	8.88 (8.88)	8.88 (8.82)	635.4

3.2.2 Thermal property of nickel complexes

Thermal property of nickel complexes were investigated using differential scanning calorimetry (DSC) and thermogravimetric analysis (TGA).

DSC thermogram of $Ni(MeOSal)_2trien$, $Ni(BuSal)_2trien$ and $Ni(diBuSal)_2trien$ in Figures 3.11, 3.13 and 3.14, respectively, showed an endotherm peak around 300, 313 and 338 °C, followed immediately by decomposition of materials. For $Ni(EtOSal)_2trien$ (Figure 3.12), DSC thermogram exhibited a large endotherm around 149°C and small endotherm around 234°C followed by decomposition of the material. These DSC data suggested that $Ni(MeOSal)_2trien$, $Ni(EtOSal)_2trien$, $Ni(BuSal)_2trien$ and $Ni(diBuSal)_2trien$ did not have liquid crystalline property.

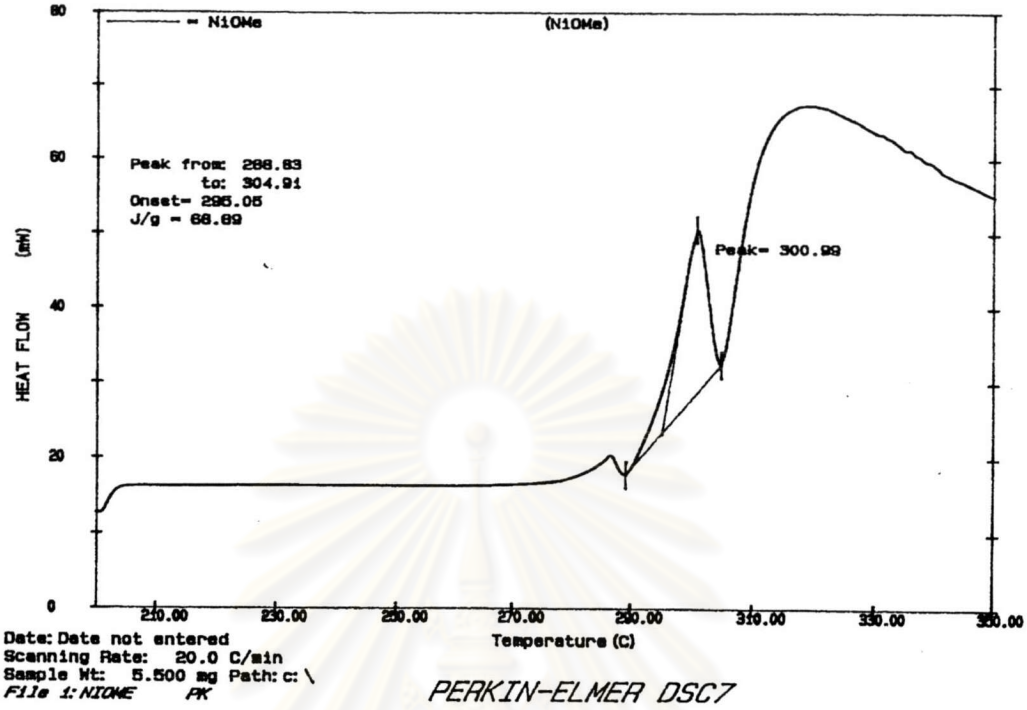

Figure 3.11 DSC thermogram of $Ni(MeOSal)_2trien$

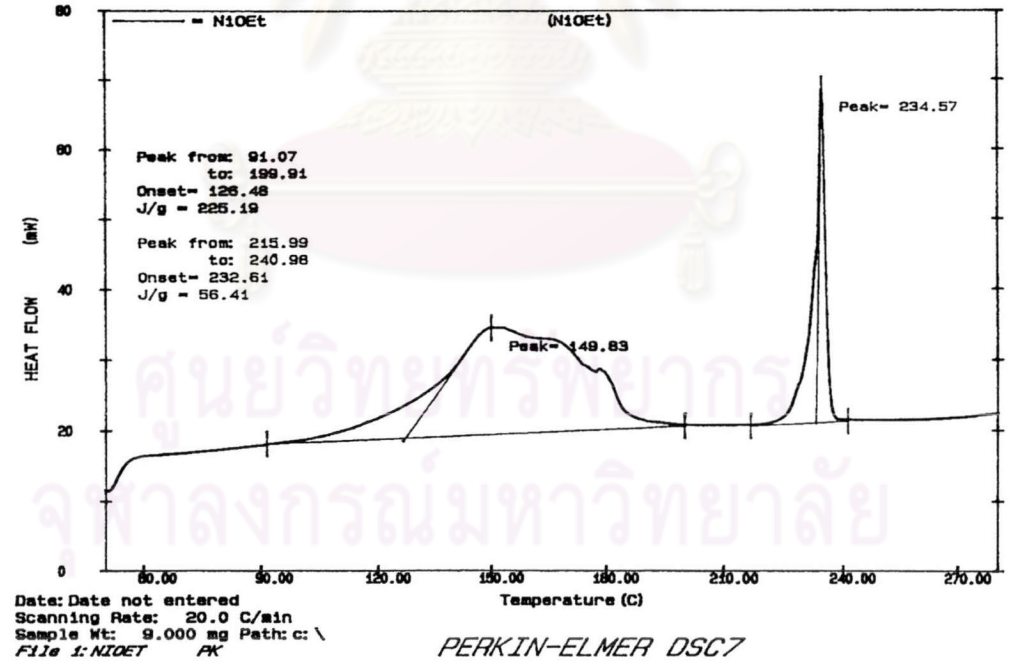

Figure 3.12 DSC thermogram of $Ni(EtOSal)_2trien$

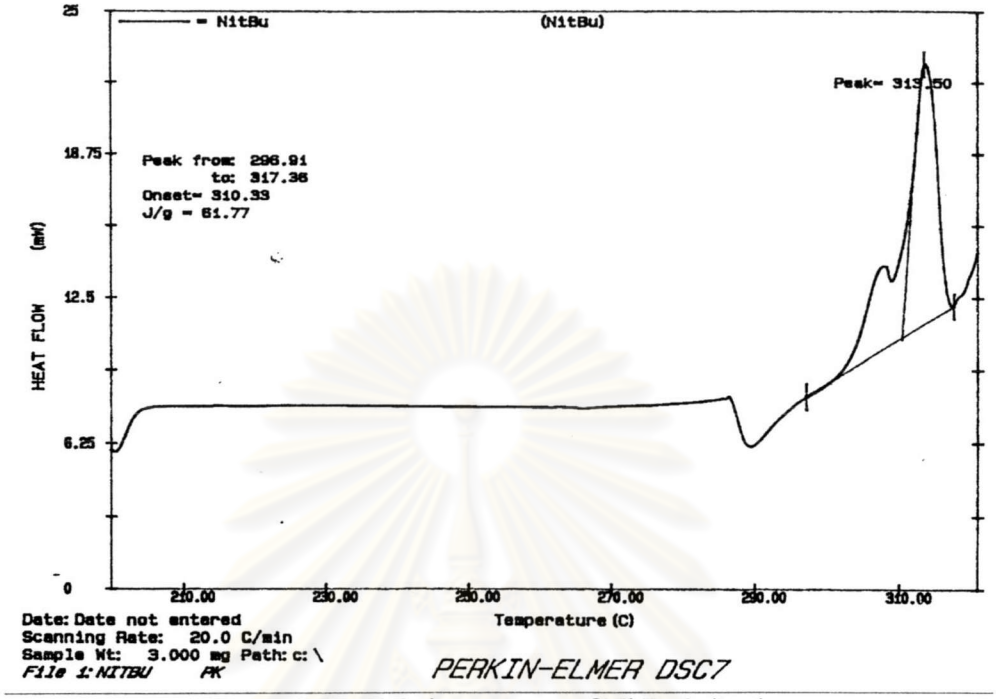

Figure 3.13 DSC thermogram of $Ni(BuSal)_2trien$

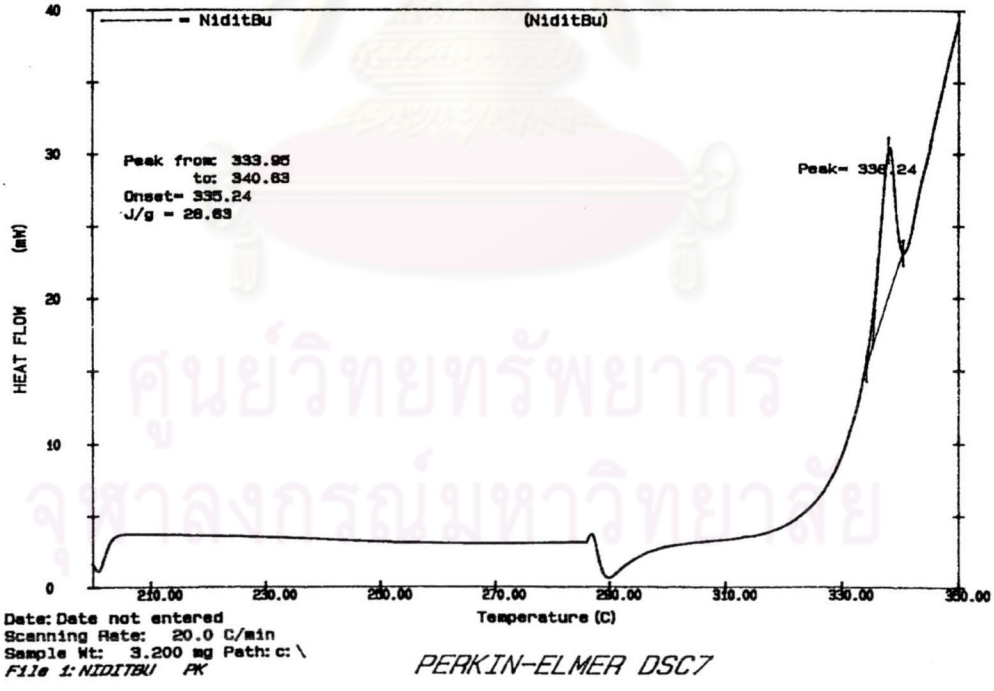

Figure 3.14 DSC thermogram of $Ni(diBuSal)_2trien$

Thermal stability of nickel complexes was studied using TGA and the thermograms are presented in Figure 3.15. The weight loss percentages of nickel complexes at different temperatures and initial decomposition temperatures are given in Table 3.6. TGA thermograms indicate that all nickel complexes were stable up to 190 °C (The initial decomposition temperature (IDT) of the nickel complexes was found to be in the range of 190-232°C.). For Ni(MeOSal)$_2$trien•H_2O and Ni(EtOSal)$_2$trien•3H_2O, the loss of solvent was not observed since TGA samples were heated in an oven at 80°C for 30 min before putting in the instrument. The residual weight percentages at 900°C of Ni(Sal)$_2$trien, Ni(MeOSal)$_2$trien, Ni(EtOSal)$_2$trien, Ni(BuSal)$_2$trien and Ni(diBuSal)$_2$trien were 20%, 16%, 18%, 10% and 12%, respectively.

Table 3.6 TGA data of nickel complexes

Nickel complexes	IDTs (°C)	Weight loss (%) at different temperature(°C)					
		300	400	500	600	700	900
Ni(Sal)$_2$trien	216	19	34	49	74	80	80
Ni(MeOSal)$_2$trien•H_2O	262	15	28	49	73	84	84
Ni(EtOSal)$_2$trien•3H_2O	186	23	40	50	71	82	82
Ni(BuSal)$_2$trien	232	12	41	61	88	89	90
Ni(diBuSal)$_2$trien	256	7	39	68	86	88	88

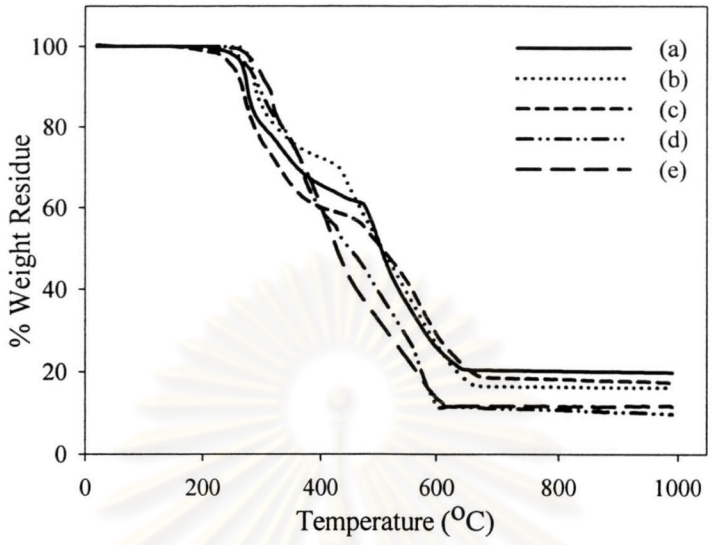

Figure 3.15 TGA thermograms of (a) $Ni(Sal)_2trien$; (b) $Ni(MeOSal)_2trien$; (c) $Ni(EtOSal)_2trien$; (d) $Ni(BuSal)_2trien$; (e) $Ni(diBuSal)_2trien$

From the thermal data described above, both zinc and nickel complexes did not showed liquid crystalline property. However, they exhibited good thermal stability. Therefore, the next step was the synthesis of polyureas containing these metal complexes in the polymer chain. These metal-containing polyureas were expected to show good thermal stability.

3.3 Synthesis of hexadentate Schiff base zinc urea complexes

The next step was to investigate the reactivity of the amine group in $Zn(Sal)_2trien$ and $Zn(XSal)_2trien$ with isocyanates to give urea group. The isocyanates employed were hexyl isocyanate, octyl isocyanate, 1,1,3,3-tetramethylbutyl isocyanate, phenyl isocyanate, benzyl isocyanate and 1-naphthyl isocyanate. This would give the information in the synthesis of metal-containing polyureas. Zinc complexes were chosen since the products could be readily characterized by NMR. The products obtained from this reaction are named as $Zn(Sal)_2trien$ urea and $Zn(XSal)_2trien$ urea.

The reaction was followed by IR spectroscopy. The completeness of the reaction was observed from the disappearance of the strong -NCO- absorption in diisocyanate at 2270 cm^{-1} and the appearance of a new -NCON- absorption band.

It was found that order of reactivity is aromatic isocyanate > aliphatic isocyanate and zinc complexes with different X group showed the relatively similar.

IR spectra of $Zn(Sal)_2$trien ureas and $Zn(XSal)_2$trien ureas (Table 3.7) showed C=N stretching bands between 1616 and 1648 cm^{-1}. The newly formed carbonyl of -NCON- group was observed in $Zn(Sal)_2$trien $urea_5$ and $Zn(diBuSal)_2$trien $urea_4$ at 1705 and 1706 cm^{-1}, respectively. The urea carbonyl in the other urea derivatives could not be observed since it overlaps with the C=N band that results in a broad absorption band.

In general, -NCON- carbonyl absorption should appear at 1660 cm^{-1}. However, $Zn(Sal)_2$trien ureas and $Zn(XSal)_2$trien ureas showed this urea carbonyl peak at 1705 and 1706 cm^{-1} because one of urea nitrogen uses its lone pair electron to coordinate with metal atom and therefore this lone pair electron cannot delocalize into the carbonyl part. This might cause the urea group to behave like an amide group.

It was found that $Zn(Sal)_2$trien urea and $Zn(XSal)_2$trien urea were unstable in the air and decomposed during purification. Therefore, ^1H NMR spectra of the purified material could not be obtained. The obtained ^1H NMR spectra showed the mixture of products and starting materials. Elemental analysis of $Zn(Sal)_2$trien ureas and $Zn(XSal)_2$trien ureas from crude reaction mixture were obtained. Most of them showed experimentally determined percentage values of carbon, hydrogen and nitrogen within the calculated values (Table 3.8).

Table 3.7 IR data of $ZnSal_2$trien ureas and $Zn(XSal)_2$trien ureas

Zinc Complex ureas	IR (cm^{-1})			
	ν_{N-H}	$\nu_{C=O}$	$\nu_{C=N}$	$\nu_{C=C}$
$Zn(Sal)_2$trien $urea_1$	3331	-	1621	1576
$Zn(Sal)_2$trien $urea_2$	3332	-	1627	1574
$Zn(Sal)_2$trien $urea_3$	3366	-	1634	1555
$Zn(Sal)_2$trien $urea_4$	3426	-	1623	1600
$Zn(Sal)_2$trien $urea_5$	3319	1705	1629	1569
$Zn(Sal)_2$trien $urea_6$	3429	-	1633	1553
$Zn(MeOSal)_2$trien $urea_1$	3333	-	1626	1572
$Zn(MeOSal)_2$trien $urea_2$	3333	-	1620	1576
$Zn(MeOSal)_2$trien $urea_3$	3294	-	1625	1544
$Zn(MeOSal)_2$trien $urea_4$	3312	-	1632	1538
$Zn(EtOSal)_2$trien $urea_1$	3332	-	1621	1576
$Zn(EtOSal)_2$trien $urea_2$	3333	-	1633	1567
$Zn(EtOSal)_2$trien $urea_3$	3324	-	1648	1597
$Zn(EtOSal)_2$trien $urea_4$	3275	-	1637	1556
$Zn(diBuSal)_2$trien $urea_1$	3332	-	1622	1577
$Zn(diBuSal)_2$trien $urea_2$	3332	-	1616	1576
$Zn(diBuSal)_2$trien $urea_3$	3370	-	1630	1549
$Zn(diBuSal)_2$trien $urea_4$	3302	1706	1625	1540
$Zn(diBuSal)_2$trien $urea_5$	3325	-	1626	1573
$Zn(diBuSal)_2$trien $urea_6$	3426	-	1629	1534

Table 3.8 Analytical data of some $Zn(Sal)_2$trien ureas and $Zn(XSal)_2$trien ureas

Zinc complex ureas	Formula (molecular weight)	Analytical data found (calculated) (%)		
		C	H	N
$Zn(Sal)_2$trien $urea_1$	$C_{34}H_{50}N_6O_4Zn$	60.73	7.58	12.43
	(672.19)	(60.75)	(7.50)	(12.50)
$Zn(Sal)_2$trien $urea_2$	$C_{38}H_{58}N_6O_4Zn$	63.13	8.34	11.17
	(728.30)	(62.67)	(8.03)	(11.54)
$Zn(Sal)_2$trien $urea_3$	$C_{38}H_{58}N_6O_4Zn$	62.63	8.06	11.78
	(728.30)	(62.67)	(8.03)	(11.54)
$Zn(Sal)_2$trien $urea_4$	$C_{34}H_{34}N_6O_4Zn$	61.93	5.27	12.85
	(656.06)	(62.24)	(5.22)	(12.81)
$Zn(MeOSal)_2$trien $urea_1$	$C_{36}H_{54}N_6O_6Zn$	59.05	7.55	11.17
	(732.24)	(59.05)	(7.43)	(11.48)
$Zn(MeOSal)_2$trien $urea_2$	$C_{40}H_{62}N_6O_6Zn$	60.84	7.90	10.83
	(788.35)	(60.94)	(7.93)	(10.66)
$Zn(diBuSal)_2$trien $urea_1$	$C_{50}H_{82}N_6O_4Zn$	65.26	9.58	9.53
	(896.61)	(65.67)	(9.26)	(9.19)
$Zn(diBuSal)_2$trien $urea_3$	$C_{54}H_{90}N_6O_4Zn$	68.01	9.72	8.95
	(952.72)	(68.08)	(9.52)	(8.82)
$Zn(diBuSal)_2$trien $urea_4$	$C_{50}H_{66}N_6O_4Zn$	68.15	7.59	9.84
	(880.49)	(68.20)	(7.56)	(9.54)

3.4 Synthesis of polyureas

3.4.1 Synthesis of metal-containing polyureas

Having obtained the synthesis data of $Zn(Sal)_2$trien ureas and $Zn(XSal)_2$trien ureas that the reaction between –NH- group in zinc complex and isocyanate could be done in refluxing methylene chloride. Therefore, this condition was employed in the synthesis of metal-containing polyureas.

Polyureas were synthesized from the reaction between $M(Sal)_2$trien or $M(XSal)_2$trien and diisocyanates (Scheme 3.2). The diisocyanates used were hexamethylene diisocyanate (HDI) and 4,4′-diphenylmethane diisocyanate (MDI). The reaction of metal complexes with diisocyanates for polyureas synthesis was done at the mole ratio of diisocyanate : $M(XSal)_2$trien = 1:1 to avoid crosslinking of the polymers. The yield of zinc-containing polyureas was in the range of 49-86%. The yield of nickel-containing polyureas was in the range of 57-79%. Zinc- and nickel-containing polyureas were obtained as yellow and yellow-brown powder, respectively.

The progress of reaction was followed by IR spectroscopy. The reaction progress could be observed by the disappearance of the strong -NCO- absorption in diisocyanate at 2270 cm^{-1} and the appearance of a new –NCON- absorption band from reaction of –NH group in metal complexes with –NCO- group at 1687-1720 cm^{-1}.

It was found that order of reactivity MDI higher than HDI. Nickel complexes is more reactive than zinc complexes and the order of reactivity of zinc and nickel complexes in different X group in metal complex is about the same.

As an example, Figure 3.18 shows the IR spectrum of the reaction products between $Ni(diBuSal)_2$trien and HDI at different reaction times. After heating the reaction for 4 hours, there was a presence of a new carbonyl (C=O) stretching vibration of –NCON- group at 1687 cm^{-1}. The completeness of polymerization was supported by the absence of the NCO peak at 2270 cm^{-1} after heating for 8 hours.

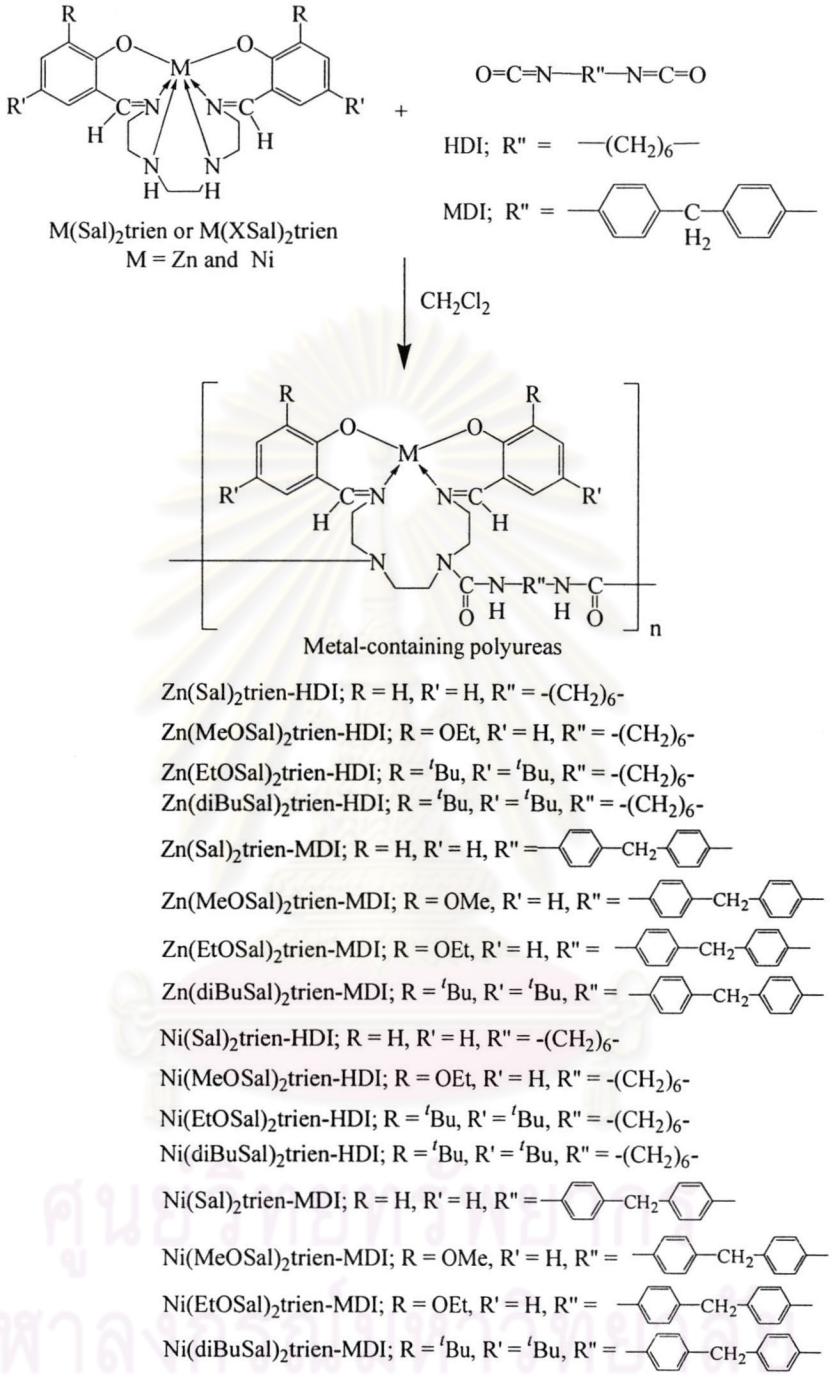

Scheme 3.2 Synthesis of polyureas from the reactions between metal complexes and diisocyanates

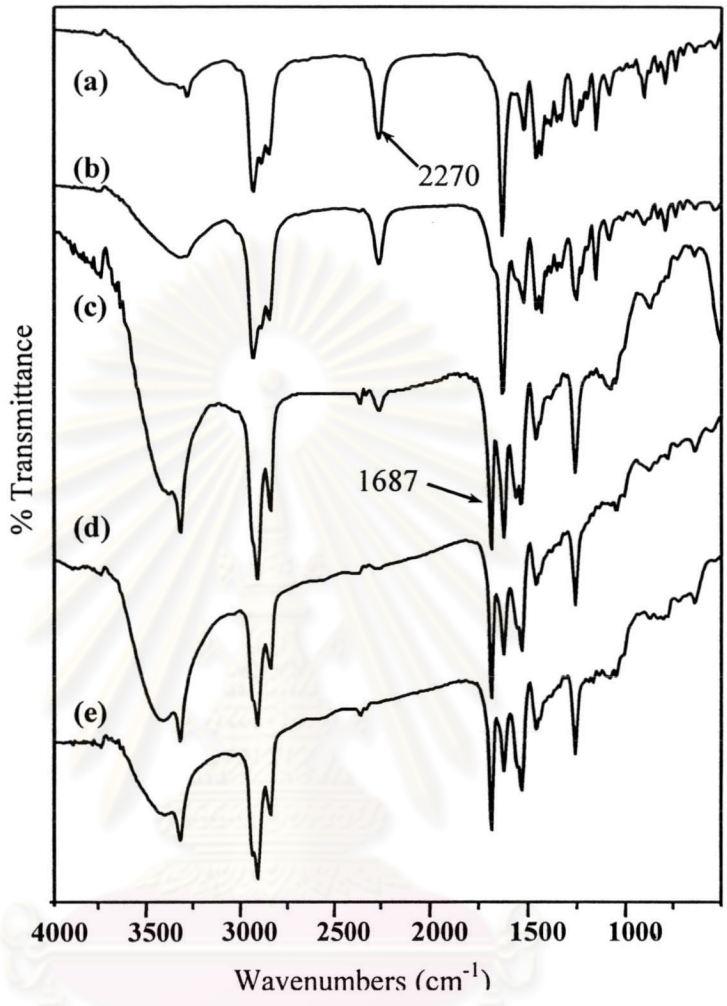

Figure 3.16 IR spectra of the reaction mixture of $Ni(diBuSal)_2trien$ with HDI at different times (a) 0 hr. (b) after 2 hr. (c) after 4 hr. (d) after 6 hr. (e) after 8 hr.

3.4.2 Characterization of metal-containing polyureas

3.4.2.1 IR spectroscopy

IR spectra of zinc- and nickel-containing polyureas are shown in Figure 3.17 and 3.18, respectively. Table 3.9 shows IR absorption bands of the polymers. All polymers showed N-H band of the urea group between 3300-3400 cm^{-1}. The C-H stretching signals appeared between 2980-2850 cm^{-1} and the carbonyl (C=O) stretching vibration of –NCON- group appeared around 1680-1720 cm^{-1}. The imine (C=N) absorption band was observed around 1620-1640 cm^{-1}.

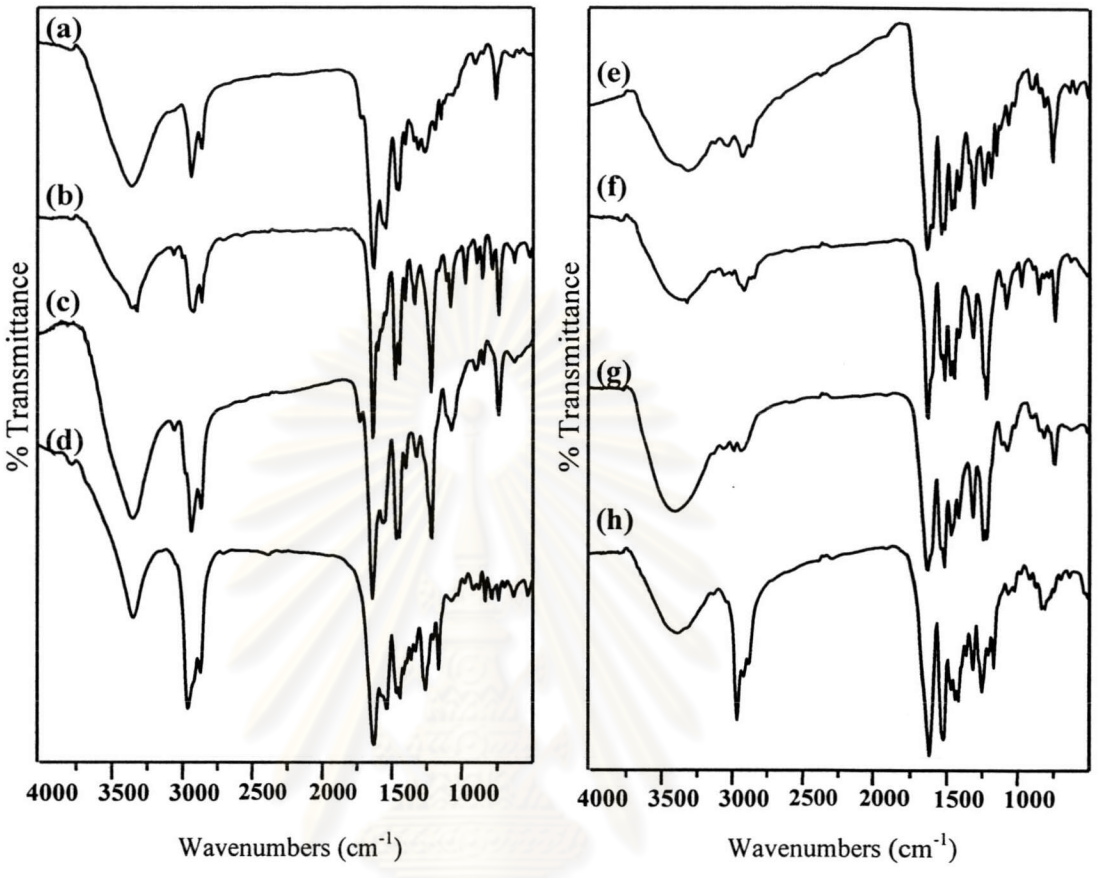

Figure 3.17 IR spectra of zinc-containing polyureas: (a) $Zn(Sal)_2$trien-HDI; (b) $Zn(MeOSal)_2$trien-HDI; (c) $Zn(EtOSal)_2$trien-HDI; (d) $Zn(diBuSal)_2$trien-HDI; (e) $Zn(Sal)_2$trien-MDI; (f) $Zn(MeOSal)_2$trien-MDI; (g) $Zn(EtOSal)_2$trien-MDI; (h) $Zn(diBuSal)_2$trien-MDI

The carbonyl of –NCON- group could clearly be observed only in $Ni(diBuSal)_2$trien-MDI (Figure 3.18 h). Urea carbonyl band in other polyureas appeared as a shoulder or broad peak due to the overlapping with -C=N- absorption.

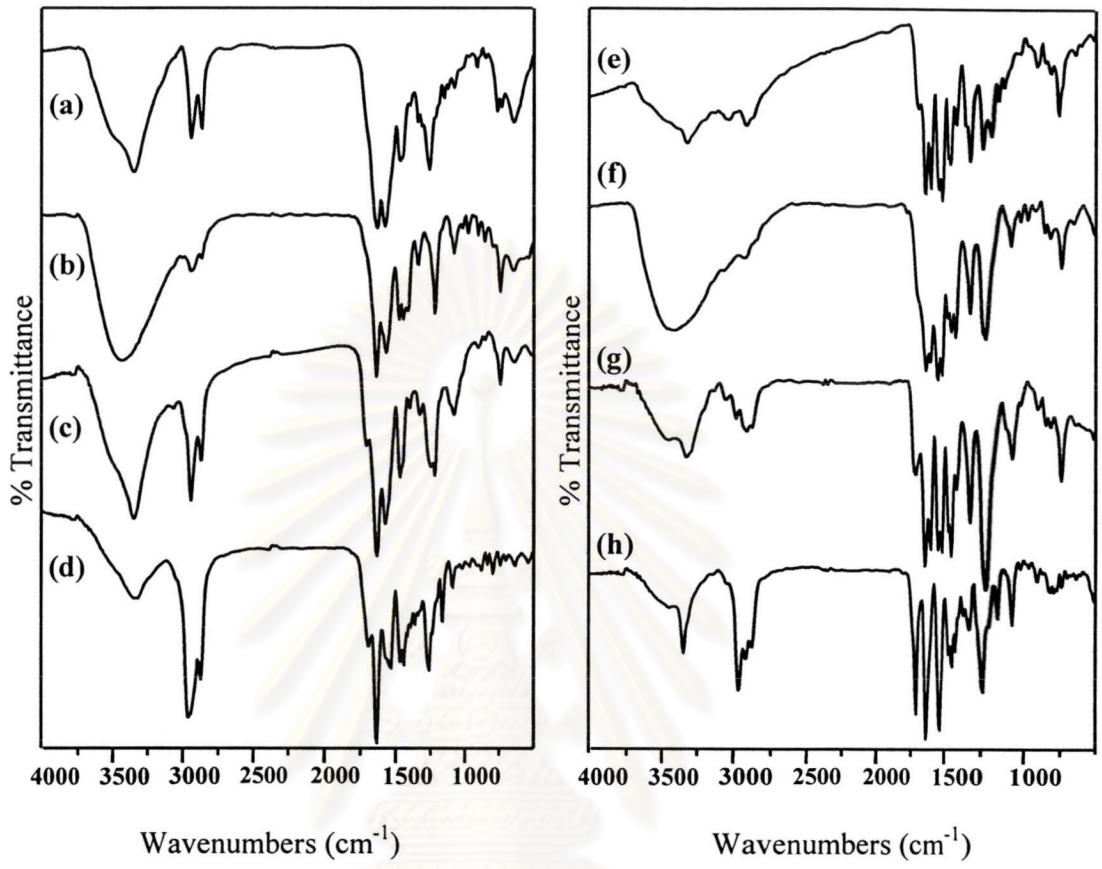

Figure 3.18 IR spectra of nickel-containing polyureas: (a) $Ni(Sal)_2$trien-HDI; (b) $Ni(MeOSal)_2$trien-HDI; (c) $Ni(EtOSal)_2$trien-HDI; (d) $Ni(diBuSal)_2$trien-HDI; (e) $Ni(Sal)_2$trien-MDI; (f) $Ni(MeOSal)_2$trien-MDI; (g) $Ni(EtOSal)_2$trien-MDI; (h) $Ni(diBuSal)_2$trien-MDI

Table 3.9 IR data of metal-containing polyureas

Polyureas	Characteristic signals
$Zn(Sal)_2$trien-HDI[b]	3348 (NH), 3048, 2950, 2929, 2857, 1720 (C=O), 1629 (C=N), 1544, 1467, 1341, 1150, 930, 759
$Zn(MeOSal)_2$trien-HDI[a]	3312 (NH), 3044, 2928, 2856, 1632 (C=N), 1565, 1473, 1446, 1335, 1217, 1078, 972, 854, 741
$Zn(EtOSal)_2$trien-HDI[b]	3346 (NH), 3039, 2927, 2859, 1719 (C=O), 1634 (C=N), 1550, 1463, 1398, 1214, 1071, 850, 741
$Zn(diBuSal)_2$trien-HDI[a]	3337 (NH), 3034, 2951, 2863, 1624 (C=N), 1531, 1457, 1437, 1257, 1162, 834, 789, 741, 636
$Zn(Sal)_2$trien-MDI[b]	3339 (NH), 3027, 2914, 1703 (C=O), 1632 (C=N), 1514, 1466, 1238, 1150, 903, 760
$Zn(MeOSal)_2$trien-MDI[a]	3310 (NH), 3039, 2982, 2906, 2823, 1630 (C=N), 1513, 1470, 1445, 1312, 1216, 1078, 972, 853, 741
$Zn(EtOSal)_2$trien-MDI[a]	3308 (NH), 3042, 2924, 2854, 1631 (C=N), 1536, 1446, 1316, 1219, 1072, 970, 853, 739
$Zn(diBuSal)_2$trien-MDI[a]	3362 (NH), 3027, 2953, 2895, 2853, 1617 (C=N), 1518, 1464, 1414, 1311, 1250, 1165, 831
$Ni(Sal)_2$trien-HDI[a]	3333 (NH), 2930, 2857, 1628 (C=N), 1573, 1466, 1258, 1158, 1079, 912, 761, 731, 644.
$Ni(MeOSal)_2$trien-HDI[a]	3423 (NH), 2930, 2847, 1632 (C=N), 1564, 1473, 1442, 1337, 1216, 1079, 976, 853, 740, 643
$Ni(EtOSal)_2$trien-HDI[b]	3337 (NH), 3044, 2930, 2853, 1701 (C=O), 1628 (C=N), 1570, 1465, 1324, 1217, 1078, 894, 740
$Ni(diBuSal)_2$trien-HDI[b]	3310 (NH), 2949, 2862, 1687 (C=O), 1630 (C=N), 1530, 1462, 1436, 1259, 1160, 1090, 877, 793, 739
$Ni(Sal)_2$trien-MDI[a]	3309 (NH), 3019, 2903, 1693 (C=O), 1639 (C=N), 1598, 1536, 1511, 1449, 1407, 1310, 1233, 1188, 1149, 1121, 907, 813, 757
$Ni(MeOSal)_2$trien-MDI[b]	3417 (NH), 2901, 1633 (C=N), 1601, 1544, 1512, 1442, 1411, 1311, 1219, 1079, 971, 740
$Ni(EtOSal)_2$trien-MDI[b]	3308 (NH), 3034, 2962, 2902, 1709 (C=O), 1640 (C=N), 1599, 1540, 1513, 1442, 1407, 1311, 1217, 1071, 903, 741
$Ni(diBuSal)_2$trien-MDI	3431, 3333 (NH), 3029, 2952, 2904, 2867, 1707 (C=O), 1631(C=N), 1528, 1461, 1437, 1314, 1234, 1158, 1072, 909, 791

[a]Urea carbonyl peak was not observed since it overlaps with C=N absorption which results in a broad peak

[b]Urea carbonyl peak was observed as a shoulder

3.4.2.2 ^{1}H NMR spectroscopy

^{1}H NMR spectra of zinc-containing polyureas were recorded in DMSO-d_6 and their characteristic signals are presented in Table 3.10 and Figure A.9-A.16.

^{1}H NMR spectra showed the characteristic imine –CH=N- protons of $Zn(Sal)_2$trien and $Zn(XSal)_2$trien between δ 8.25-8.21. The aromatic region signals showed 4 multiplets due to unsymmetrical structure of metal complex as follows: δ 7.36-7.33, 7.12-7.05, 6.88-6.79, 6.50-6.48. The aliphatic protons of HDI showed signals at δ 1.35-1.37 and 1.24. The aliphatic region of complex in the region δ 2.4-3.6 could not be clearly observed due to large peaks of H_2O in DMSO-d_6 and therefore the chemical shift that could be clearly observed is mainly in the aromatic region. All zinc-containing polymers show aromatic peaks due to the metal complex in a similar pattern to those observed in the metal complex itself. An example of NMR spectra in the aromatic region of $Zn(EtOSal)_2$trien and $Zn(EtOSal)_2$trien-MDI in $CDCl_3$ and DMSO-d_6, respectively. The aromatic peaks in $Zn(EtOSal)_2$trien were observed at δ 6.66 (2H, *d*, Ar-H, J = 8 Hz), 6.62 (2H, *d*, Ar-H, J = 8 Hz), 6.21 (2H, *t*, Ar-H, J = 7.6 Hz), and these protons were also found in $Zn(EtOSal)_2$trien-MDI at δ 6.71 (2H, *d*, Ar-H, J = 8.0 Hz), 6.61 (2H, *d*, Ar-H, J = 6.8 Hz), 6.09 (2H, *t*, Ar-H, J = 7.6 Hz). The CH=N was observed as singlet in both $Zn(EtOSal)_2$trien and $Zn(EtOSal)_2$trien-MDI at δ 8.12 and 8.25, respectively. The aromatic peaks due to MDI were observed in $Zn(EtOSal)_2$trien-MDI at 7.32-7.36 (2H, *m*, Ar-H), 7.06-7.12 (2H, *m*, Ar-H), 6.79-6.86 (2H, *m*, Ar-H), 6.48-6.50 (2H, *m*, Ar-H).

Table 3.10 ^{1}H NMR data of polyureas

Polyureas	Characteristic signals
Zn(Sal)$_2$trien-HDI	8.25 (2H, *s*, C<u>H</u>=N), 7.03 (2H, *d*, Ar-<u>H</u>, *J* = 7.6 Hz), 6.95 (2H, *t*, Ar-<u>H</u>, *J* = 8.0 Hz), 6.32 (2H, *d*, Ar-<u>H</u>, *J* = 8 Hz), 6.23 (2H, *t*, Ar-<u>H</u>, *J* = 7.6 Hz), 5.81 (2H, *m*, N<u>H</u>), 1.36 (4H, *br*, C<u>H</u>$_2$), 1.24 (4H, *br*, C<u>H</u>$_2$)
Zn(MeOSal)$_2$trien-HDI	8.25 (2H, *s*, C<u>H</u>=N), 6.69 (2H, *dd*, Ar-<u>H</u>, *J* = 1.6, 8.0 Hz), 6.61 (2H, *dd*, Ar-<u>H</u>, *J* = 1.2, 7.6 Hz) 6.13 (2H, *t*, Ar-<u>H</u>, *J* = 7.6 Hz) 5.80 (2H, *m*, N<u>H</u>), 3.59 (6H, *s*, OC<u>H</u>$_3$), 1.37 (4H, *br*, C<u>H</u>$_2$), 1.24 (4H, *br*, C<u>H</u>$_2$)
Zn(EtOSal)$_2$trien-HDI	8.25 (2H, *s*, C<u>H</u>=N), 6.71 (2H, *dd*, Ar-<u>H</u>, *J* = 1.6, 8.0 Hz), 6.61(2H, *dd*, Ar-<u>H</u>, *J* = 1.6, 8.0 Hz), 6.09 (2H, *t*, Ar-<u>H</u>, *J* = 7.6 Hz), 5.82 (2H, *m*, N<u>H</u>), 3.74-3.89 (4H, *m*, OC<u>H</u>$_2$), 1.35 (4H, *br*, C<u>H</u>$_2$), 1.24 (4H, *br*, C<u>H</u>$_2$), 1.10 (6H, *t*, C<u>H</u>$_3$, *J* = 6.8 Hz)
Zn(diBuSal)$_2$trien-HDI	8.21 (2H, *s*, C<u>H</u>=N), 6.99 (2H, *d*, Ar-<u>H</u>, *J* = 2.8 Hz), 6.76 (2H, *d*, Ar-<u>H</u>, *J* = 2.4 Hz), 5.81 (2H, *m*, N<u>H</u>), 1.37-1.31 (8H, *m*, C<u>H</u>$_2$), 1.22 (9H, *s*, C<u>H</u>$_3$), 1.80 (9H, *s*, C<u>H</u>$_3$)
Zn(Sal)$_2$trien-MDI	8.25 (2H, *s*, C<u>H</u>=N), 7.33-7.36 (2H, *m*, Ar-<u>H</u>), 7.05-7.12 (2H, *m*, Ar-<u>H</u>), 7.03 (2H, *d*, Ar-<u>H</u>, *J* = 7.2 Hz), 6.95 (2H, *t*, Ar-<u>H</u>, *J* = 7.6 Hz), 6.86-6.88 (2H, *m*, Ar-<u>H</u>), 6.48-6.50 (2H, *m*, Ar-<u>H</u>), 6.32 (2H, *d*, Ar-<u>H</u>, *J* = 8.8 Hz), 6.23 (2H, *t*, Ar-<u>H</u>, *J* = 7.2 Hz)
Zn(MeOSal)$_2$trien-MDI	8.25 (2H, *s*, C<u>H</u>=N), 7.32-7.36 (2H, *m*, Ar-<u>H</u>), 7.06-7.12 (2H, *m*, Ar-<u>H</u>), 6.81-6.87 (2H, *m*, Ar-<u>H</u>), 6.69 (2H, *dd*, Ar-<u>H</u>, *J* = 1.6, 7.6 Hz), 6.61 (2H, *dd*, Ar-<u>H</u>, *J* = 1.6, 7.2 Hz), 6.48-6.50 (2H, *m*, Ar-<u>H</u>), 6.14 (2H, *t*, Ar-<u>H</u>, *J* = 7.6 Hz), 3.59 (6H, *s*, OC<u>H</u>$_3$)
Zn(EtOSal)$_2$trien-MDI	8.25 (2H, *s*, C<u>H</u>=N), 7.32-7.36 (2H, *m*, Ar-<u>H</u>), 7.06-7.12 (2H, *m*, Ar-<u>H</u>), 6.79-6.86 (2H, *m*, Ar-<u>H</u>), 6.71 (2H, *dd*, Ar-<u>H</u>, *J* = 1.6, 8.0 Hz), 6.61 (2H, *dd*, Ar-<u>H</u>, *J* = 1.6, 6.8 Hz), 6.48-6.50 (2H, *m*, Ar-<u>H</u>), 6.09 (2H, *t*, Ar-<u>H</u>, *J* = 7.6 Hz), 3.74-3.89 (4H, *m*, OC<u>H</u>$_2$), 1.10 (6H, *t*, C<u>H</u>$_3$, *J* = 6.8 Hz)
Zn(diBuSal)$_2$trien-MDI	8.43 (1H, *s*, C<u>H</u>=N), 8.29 (1H, *s*, C<u>H</u>=N), 6.70-7.46 (10H, *m*, Ar-<u>H</u>), 6.50-6.54(2H, *m*, Ar-<u>H</u>), 1.22-1.32 (36H, *s*, C<u>H</u>$_3$)

3.4.2.3 Elemental analysis

The chemical structure of metal-containing polyureas was confirmed by elemental analysis. Table 3.11 and Table 3.12 show possible molecular formula of zinc- and nickel-containing polyureas, respectively. From the elemental analysis data, it was found that $Zn(MeOSal)_2$trien-HDI gave the same percentages of carbon, hydrogen and nitrogen as the calculated values.

Table 3.11 Analytical data of zinc-containing polyureas

Polyureas	Repearting unit	Analytical data found (calculated) (%)		
		C	H	N
$Zn(Sal)_2$trien-HDI	$C_{28}H_{36}N_6O_4Zn$	54.37	6.53	14.48
		(57.39)	(6.19)	(14.34)
$Zn(MeOSal)_2$trien-HDI	$C_{30}H_{40}N_6O_6Zn$	55.60	6.36	13.04
		(55.77)	(6.24)	(13.01)
$Zn(EtOSal)_2$trien-HDI	$C_{32}H_{44}N_6O_6Zn$	54.48	7.61	14.44
		(57.01)	(6.58)	(12.47)
$Zn(diBuSal)_2$trien-HDI	$C_{44}H_{68}N_6O_4Zn$	63.63	8.76	10.23
		(65.21)	(8.46)	(10.37)
$Zn(Sal)_2$trien-MDI	$C_{35}H_{34}N_6O_4Zn$	61.13	5.23	12.45
		(62.92)	(5.13)	(12.58)
$Zn(MeOSal)_2$trien-MDI	$C_{37}H_{38}N_6O_6Zn$	59.32	5.37	11.11
		(61.03)	(5.26)	(11.54)
$Zn(EtOSal)_2$trien-MDI	$C_{39}H_{42}N_6O_6Zn$	57.99	5.61	10.96
		(61.95)	(5.60)	(11.11)
$Zn(diBuSal)_2$trien-MDI	$C_{51}H_{66}N_6O_4Zn$	67.16	7.54	9.23
		(68.63)	(7.45)	(9.42)

Table 3.12 Analytical data of nickel-containing polyureas

Polyureas	Repearting unit	Analytical data found (calculated) (%)		
		C	H	N
Ni(Sal)$_2$trien-HDI	$C_{28}H_{36}N_6O_4Ni$	56.49	6.42	14.42
		(58.05)	(6.26)	(14.51)
Ni(MeOSal)$_2$trien-HDI	$C_{30}H_{40}N_6O_4Ni$	57.35	5.81	9.65
		(56.36)	(6.31)	(13.14)
Ni(EtOSal)$_2$trien-HDI	$C_{32}H_{44}N_6O_6Ni$	53.68	7.34	12.65
		(57.59)	(6.64)	(12.59)
Ni(diBuSal)$_2$trien-HDI	$C_{44}H_{68}N_6O_4Ni$	64.30	10.41	9.09
		(65.75)	(8.53)	(10.46)
Ni(Sal)$_2$trien-MDI	$C_{35}H_{34}N_6O_4Ni$	61.32	5.96	12.87
		(63.56)	(5.18)	(12.71)
Ni(MeOSal)$_2$trien-MDI	$C_{37}H_{38}N_6O_6Ni$	59.18	5.10	11.09
		(61.60)	(5.31)	(11.65)
Ni(EtOSal)$_2$trien-MDI	$C_{39}H_{42}N_6O_6Ni$	60.20	6.60	10.50
		(62.50)	(5.65)	(11.21)
Ni(diBuSal)$_2$trien-MDI	$C_{51}H_{66}N_6O_4Ni$	65.38	8.05	8.77
		(69.15)	(7.51)	(9.49)

3.4.2.4 Thermal analysis

TGA curves and weight loss data of zinc-containing polyureas obtained from zinc complexes and HDI are presented in Figure 3.19 and Table 3.13, respectively. Initial decomposition temperature (IDT) of the polyureas was found to be in the range of 220-246°C. The residual weight percentages at 900°C of Zn(Sal)$_2$trien-HDI, Zn(MeOSal)$_2$trien-HDI, Zn(EtOSal)$_2$trien-HDI and Zn(diBuSal)$_2$trien-HDI were 14%, 13%, 10% and 12%, respectively.

Possible mechanism of degradation proceeded *via* urea scission to give isocyanate and amine components (Scheme 3.3).

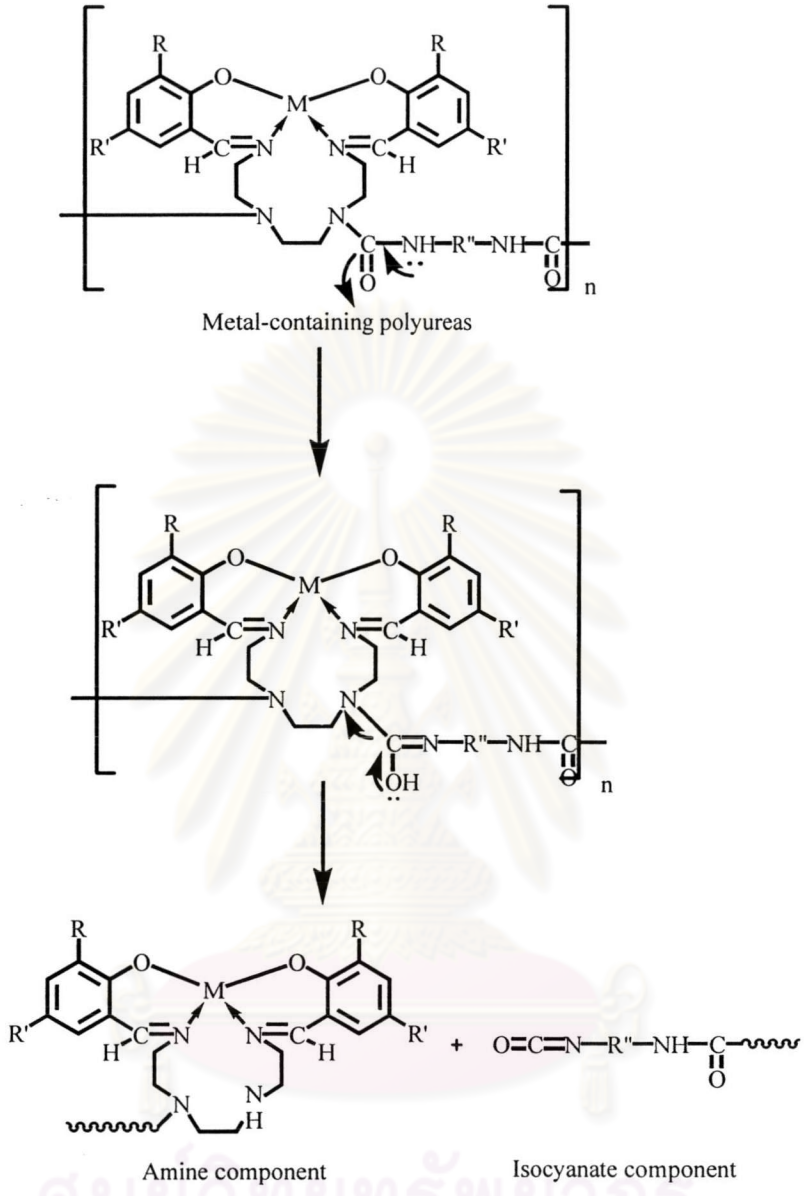

Scheme 3.3 Initial thermal degradation of metal-containing polyureas

Figure 3.20 and Table 3.14 show TGA curves and weight loss data of zinc-containing polyureas obtained from zinc complexes and MDI. Initial decomposition temperature (IDT) of the polyureas was found to be in the range of 216-260°C. The residual weight percentages at 900°C of $Zn(Sal)_2$trien-MDI, $Zn(MeOSal)_2$trien-MDI, $Zn(EtOSal)_2$trien-MDI and $Zn(diBuSal)_2$trien-MDI were 12%, 15%, 14% and 12%, respectively.

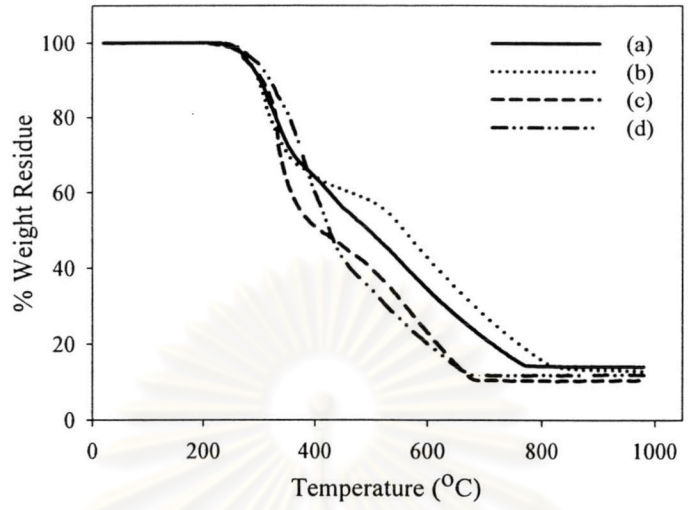

Figure 3.19 TGA thermograms of (a) $Zn(Sal)_2$trien-HDI; (b) $Zn(MeOSal)_2$trien-HDI; (c) $Zn(EtOSal)_2$trien-HDI; (d) $Zn(diBuSal)_2$trien-HDI

Table 3.13 TGA data of zinc-containing polyureas based on HDI

Zinc-containing polyureas	IDTs (°C)	Weight loss (%) at various temperature (°C)						
		300	400	500	600	700	800	900
$Zn(Sal)_2$trien-HDI	246	10	36	50	65	79	86	86
$Zn(MeOSal)_2$trien-HDI	220	11	36	42	57	73	84	87
$Zn(EtOSal)_2$trien-HDI	220	9	49	60	77	90	90	90
$Zn(diBuSal)_2$trien-HDI	242	6	40	65	80	88	88	88

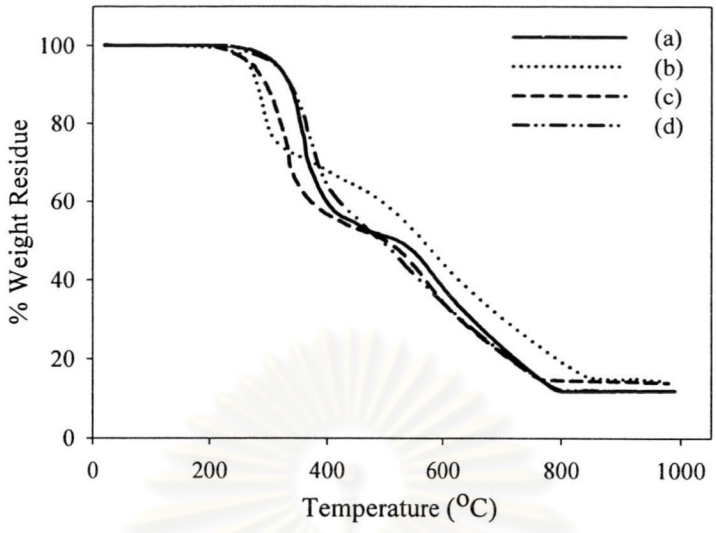

Figure 3.20 TGA thermograms of (a) $Zn(Sal)_2$trien-MDI; (b) $Zn(MeOSal)_2$trien-MDI; (c) $Zn(EtOSal)_2$trien-MDI; (d) $Zn(diBuSal)_2$trien-MDI

Table 3.14 TGA data of zinc-containing polyureas based on MDI

Zinc-containing polyureas	IDTs	Weight loss (%) at various temperature (°C)						
	(°C)	300	400	500	600	700	800	900
$Zn(Sal)_2$trien-MDI	260	3	40	49	62	77	88	88
$Zn(MeOSal)_2$trien-MDI	226	21	32	41	56	70	81	85
$Zn(EtOSal)_2$trien-MDI	216	11	43	50	66	79	86	86
$Zn(diBuSal)_2$trien-MDI	240	4	36	51	66	78	88	88

TGA curves of nickel-containing polyureas obtained from the reaction between nickel complexes and diisocyanates, HDI and MDI, were presented in Figures 3.21 and 3.22, respectively. The polymer weight loss data are shown in Tables 3.15 and 3.16. When HDI was employed as diisocyanates (Figure 3.21), initial decomposition temperature (IDT) of the polyureas was found to be in the range of 174-228°C. The residual weight of $Ni(Sal)_2$trien-HDI, $Ni(MeOSal)_2$trien-HDI, $Ni(EtOSal)_2$trien-HDI and $Ni(diBuSal)_2$trien-HDI were 7%, 20%, 11% and 13%, respectively.

When MDI was employed as diisocyanates (Figure 3.22), initial decomposition temperature (IDT) of the polyureas was found to be in the range of

190-232°C. The residual weight percentages at 900°C of Ni(Sal)$_2$trien-MDI, Ni(MeOSal)$_2$trien-MDI, Ni(EtOSal)$_2$trien-MDI and Ni(diBuSal)$_2$trien-MDI were 4%, 14%, 11% and 9%, respectively.

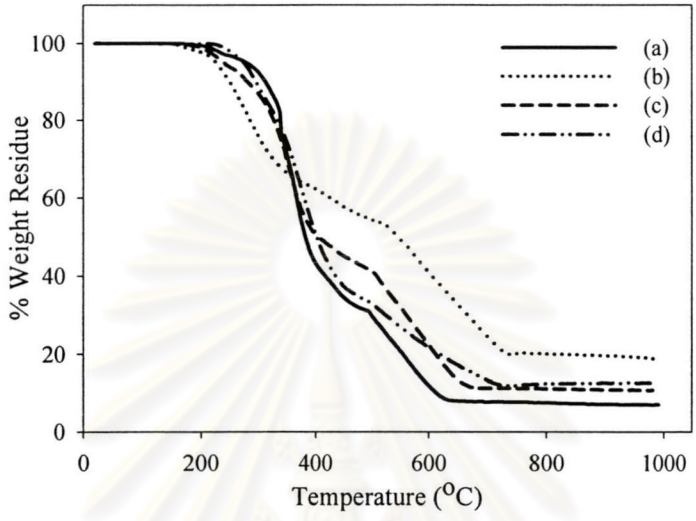

Figure 3.21 TGA thermograms of (a) Ni(Sal)$_2$trien-HDI; (b) Ni(MeOSal)$_2$trien-HDI; (c) Ni(EtOSal)$_2$trien-HDI; (d) Ni(diBuSal)$_2$trien-HDI

Table 3.15 TGA data of nickel-containing polyureas based on HDI

Nickel-containing polyureas	IDTs	Weight loss (%) at different temperature (°C)						
	(°C)	300	400	500	600	700	800	900
Ni(Sal)$_2$trien-HDI	206	8	57	70	88	92	93	93
Ni(MeOSal)$_2$trien-HDI	174	24	38	46	59	75	80	80
Ni(EtOSal)$_2$trien-HDI	180	13	49	59	76	89	89	89
Ni(diBuSal)$_2$trien-HDI	228	11	49	67	78	87	88	88

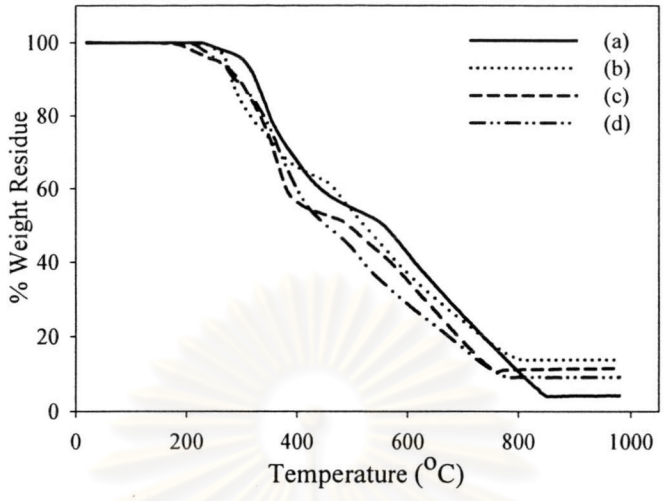

Figure 3.22 TGA thermograms of (a) Ni(Sal)$_2$trien-MDI; (b) Ni(MeOSal)$_2$trien-MDI; (c) Ni(EtOSal)$_2$trien-MDI; (d) Ni(diBuSal)$_2$trien-MDI

Among all of polyureas, the polymers obtained from Zn(MeOSal)$_2$trien and Ni(MeOSal)$_2$trien are the most thermally stable polymers. In comparison between different X groups in the metal complexes, the polymers based on Zn(diBuSal)$_2$trien showed the same thermal stability as those based on ZnSal$_2$trien.

Table 3.16 TGA data of nickel-containing polyureas based on MDI

Nickel-containing polyureas	IDTs (°C)	Weight loss (%) at different temperature (°C)						
		300	400	500	600	700	800	900
Ni(Sal)$_2$trien-MDI	232	4	32	45	57	74	89	96
Ni(MeOSal)$_2$trien-MDI	230	16	34	46	63	76	86	86
Ni(EtOSal)$_2$trien-MDI	190	11	44	51	65	81	89	89
Ni(diBuSal)$_2$trien-MDI	210	12	40	57	72	83	91	91

Comparing with the metal-free polyurea synthesis from toluene diisocyanate and 4,4′-diaminodiphenylmethane,[26] initial decomposition temperature (IDT) of the metal-free polyureas is 260°C, and the weight loss percentage at 300°C is 60%.

3.4.2.5 Solubility

Solubility of metal-containing polyureas was tested in various polar and non-polar solvents (Table 3.17).

Table 3.17 Solubility of metal-containing polyureas[a]

Polyureas	THF	DMF	DMSO
Zn(Sal)$_2$trien-HDI	-	-	+
Zn(MeOSal)$_2$trien-HDI	-	-	+
Zn(EtOSal)$_2$trien-HDI	-	-	+
Zn(diBuSal)$_2$trien-HDI	-	-	+
Zn(Sal)$_2$trien-MDI	-	-	+
Zn(MeOSal)$_2$trien-MDI	-	-	+
Zn(EtOSal)$_2$trien-MDI	-	-	+
Zn(diBuSal)$_2$trien-MDI	+	++	+
Ni(Sal)$_2$trien-HDI	-	-	+
Ni(MeOSal)$_2$trien-HDI	-	-	+
Ni(EtOSal)$_2$trien-HDI	-	-	+
Ni(diBuSal)$_2$trien-HDI	-	-	+
Ni(Sal)$_2$trien-MDI	-	+	+
Ni(MeOSal)$_2$trien-MDI	-	-	+
Ni(EtOSal)$_2$trien-MDI	-	++	+
Ni(diBuSal)$_2$trien-MDI	++	++	+

-, Insoluble; +, Soluble on heating; ++, Soluble

[a] 10 mg sample was dissolved in 2 ml of a solvent.

All metal-containing polyureas are soluble in DMSO but insoluble in *n*-hexane, toluene, diethyl ether, chloroform, methanol and water. The polymers obtained from metal complexes with good solubility such as Zn(diBuSal)$_2$trien are also soluble in less polar solvents. It was found that Zn(diBuSal)$_2$trien-MDI, Ni(Sal)$_2$trien-MDI, Ni(EtOSal)$_2$trien-MDI and Ni(diBuSal)$_2$trien-MDI are soluble in DMF. Zn(diBuSal)$_2$trien-MDI and Ni(diBuSal)$_2$trien-MDI are soluble in THF.

3.4.2.6 Inherent viscosity

The inherent viscosity of all polyureas was measured at 40°C in DMSO. The viscosity data of metal-containing polyureas are given in Table 3.18.

Ni-containing polyureas showed the same viscosity as Zn-containing polyureas when the polymers were prepared from metal complex with the same ligand

and diisocyanate. In comparison between the polymer obtained from different metal complexes, the inherent viscosity increases in the order of $M(diBuSal)_2trien$ > $M(MeOSal)_2trien$ = $M(EtOSal)_2trien$ > $M(Sal)_2trien$.

From the work of Wang,[26] the viscosity of metal-containing polyureas was found to be in the range between 0.04-0.41 dL/g. To compare with metal free polyurea, the result showed that the inherent viscosity of metal free polyurea is 0.60 dL/g which higher than those of the metal-containing polyureas.

Table 3.18 Inherent viscosity of metal-containing polyureas

Polymers	η_{inh}(dL/g)[a]	Polymers	η_{inh}(dL/g)[a]
$Zn(Sal)_2trien$-HDI	0.1731	$Ni(Sal)_2trien$-HDI	0.1410
$Zn(MeOSal)_2trien$-HDI	0.1822	$Ni(MeOSal)_2trien$-HDI	0.1212
$Zn(EtOSal)_2trien$-HDI	0.2428	$Ni(EtOSal)_2trien$-HDI	0.1932
$Zn(diBuSal)_2trien$-HDI	0.3299	$Ni(diBuSal)_2trien$-HDI	0.3101
$Zn(Sal)_2trien$-MDI	0.1806	$Ni(Sal)_2trien$-MDI	0.1177
$Zn(MeOSal)_2trien$-MDI	0.2428	$Ni(MeOSal)_2trien$-MDI	0.2198
$Zn(EtOSal)_2trien$-MDI	0.2766	$Ni(EtOSal)_2trien$-MDI	0.3000
$Zn(diBuSal)_2trien$-MDI	0.3497	$Ni(diBuSal)_2trien$-MDI	0.3456

[a] determined at a concentration of 0.5 g/100 ml in DMSO at 40°C

3.4.2.7 Flame-retardancy

Flame-retardant properties of metal-containing polyureas were compared from their limiting oxygen index (LOI) values as shown in Table 3.19. Limiting oxygen index (LOI) is the minimum concentration of oxygen, expressed as volume percent, in a mixture of oxygen and nitrogen that will support flaming combustion of a material. LOI measurement was carried out as described in appendix C-1. A polymer having an LOI greater than 21 does not burn in atmosphere since the oxygen content in atmosphere is 21%. The polymer with higher LOI is more flame retardant. LOI value of the polymers were in the range of 23-36. The LOI data of $ZnSal_2trien$-based polyureas are equal to those of $NiSal_2trien$-based polyureas. The metal-containing polyureas based on MDI show slightly higher flame retardancy than those derived from HDI because of the presence of aromatic rings in the main chain of the polymer.

In comparison to the previous work reported by Nanjundan,[35] the obtained polymers exhibited higher LOI values in the range between 27 to 36.

Table 3.19 LOI data of metal-containing polyureas

Polymers	LOI	Polymers	LOI
$Zn(Sal)_2$trien-HDI	23.5	$Ni(Sal)_2$trien-HDI	23.7
$Zn(MeOSal)_2$trien-HDI	32.5	$Ni(MeOSal)_2$trien-HDI	33.7
$Zn(EtOSal)_2$trien-HDI	32.8	$Ni(EtOSal)_2$trien-HDI	33.5
$Zn(diBuSal)_2$trien-HDI	32.5	$Ni(diBuSal)_2$trien-HDI	30.4
$Zn(Sal)_2$trien-MDI	24.7	$Ni(Sal)_2$trien-MDI	24.8
$Zn(MeOSal)_2$trien-MDI	33.6	$Ni(MeOSal)_2$trien-MDI	34.9
$Zn(EtOSal)_2$trien-MDI	34.8	$Ni(EtOSal)_2$trien-MDI	34.5
$Zn(diBuSal)_2$trien-MDI	36.4	$Ni(diBuSal)_2$trien-MDI	33.4